Investigation of MgO as a candidate for the primary nucleating dust species around M stars

Jayesh S. Bhatt★† and Ian J. Ford

Department of Physics and Astronomy, University College London, Gower Street, London WC1E 6BT

ABSTRACT

The possibility of magnesium oxide being the first species to nucleate in the cooling outflows around M stars has been investigated. By treating the formation of the seed nuclei as a homogeneous nucleation problem and using molecular dynamics data obtained with the 'compressible ion potential' for MgO, free energy calculations are performed to obtain an estimate of the population densities of MgO clusters of various sizes. It is found that a free energy barrier of at least hundreds of $k_B T$ would need to be climbed in order for MgO to nucleate in significant amount in typical circumstellar shells, hence ruling out MgO as a realistic candidate for the primary nucleating dust species. This is in agreement with a similar conclusion reached in earlier studies, although the present calculations are based on a much more robust potential model for MgO.

Key words: astrochemistry – circumstellar matter.

1 INTRODUCTION

Dust particles play a crucial catalytic role in interstellar chemistry, heterogeneous mantle growth and in the overall process of star formation. The dust particles themselves, however, are very unlikely to form in the ultralow density conditions of the interstellar medium (ISM). Calculations based on stochastic chemical kinetics have shown that the formation of molecules (Green et al. 2001; Lushnikov, Bhatt & Ford 2003), or the nucleation of small molecular clusters (Bhatt & Ford 2003), in interstellar conditions even with the help of a catalyzing surface is far more difficult than earlier studies based on classical chemical kinetics suggested. The painstakingly long chain of reactions required to form a macroscopic dust grain from an unstable phase may be so slow in the ISM that the cluster would most likely disintegrate before it becomes a stable grain. For clusters to grow to radii of 10^{-7} m under typical interstellar conditions, the time-scale required would be in terms of billions of years (Dyson & Williams 1997), that is, comparable to the age of the Universe, hence ruling out the ISM as a potential place of origin for cosmic dust grains.

Instead, the process of dust formation is thought to take place well before the material is expelled in the ISM, in the denser regions of circumstellar shells around stars that have completed one full life-cycle and are losing material rapidly due to thermal pulsation. The relatively high temperatures around stars ($\sim 10^3$ K) also provide the ideal condition for gaseous atoms to fall into the most-stable molecular states before participating in dust formation. The possibility of

stellar atmospheres as regions for nucleation of stardust was first pointed out in 1962 by Hoyle & Wickramasinghe (1962).

Among the variety of objects whose environments are conducive to dust formation, late-type giants and supergiants offer a unique combination of advantages when concerned with the study of dust formation. They are quite numerous in the sky and their mass-loss rate is very high; estimates suggest (van Loon et al. 1999; Habing & Olofsson 2003) that for very luminous red giants and supergiants, the mass-loss rate can be as high as $10^{-4} \, M_\odot \, yr^{-1}$, where $M_\odot$ denotes the mass of the Sun. This is an enormously large value when one notes that for the Sun, for example, the current mass-loss rate is only about $2 \times 10^{-14} \, M_\odot \, yr^{-1}$. In total, late-type giants are thought to eject more than $0.3 \, M_\odot \, yr^{-1}$ of material into the ISM in our Galaxy (Tielens, Waters & Bernatowicz 2005). Unlike nova outbursts, giants and supergiants do not exhibit any strong source of ultraviolet (UV) radiation; chromospheres in giants may exhibit weak UV radiation, but it may be neglected in order to avoid additional complexity in chemistry calculations. Also, since circumstellar shells around late-type giants such as M stars are a significant source of infrared and microwave emission, these objects are observationally quite well studied. It is therefore sensible to study the problem of dust formation around these objects.

Dust chemistry environments are generally classified into two types: oxygen rich and carbon rich. While carbonaceous grain formation has been studied with quite a lot of success and the associated chemical pathway is relatively well defined (Gail & Sedlmayr 1985, 1987, 1988), this is not the case for inorganic dust formation around M stars (Cherchneff 2006). The overall chemical composition of dust in oxygen-rich clouds may be inferred through observations, but identifying the primary condensing material, which generally lies hidden at the core of the dust particles, has proved to be less than straightforward. Interpretation of spectral features of the

---

★E-mail: bhatt@physics.org
†Present address: Imperial College London, Exhibition Road, London SW7 2AZ.

interstellar grains with the help of laboratory experiments (Begemann et al. 1995; Colangeli et al. 2003; Molster & Waters 2003; Whittet 2003) has brought about widespread acceptance that the main constituents of dust around M stars are amorphous silicates. However, it has been argued that they cannot be the material directly nucleating from the gas phase, since the first few steps of the formation of dimers, trimers, etc., are chemically untenable (Gail & Sedlmayr 1987). It is also believed that the most-abundant monomeric species that could facilitate the production of dust are Fe, Mg, SiO and H_2O. Among these, the SiO molecule has a high bond energy ($\sim$8.3 eV). One popular belief was that SiO crystals nucleate first and then all these four species get involved in further growth of the particle. This scenario was, however, questioned on the grounds that the major condensation phase typically occurs around late-type M stars within the temperature range of 800–1200 K and the nucleation temperature required for SiO would be 600 K or less (Nuth & Donn 1982, 1983; Gail & Sedlmayr 1986, 1998).

Earlier, a possibility was discussed that iron–magnesium oxides may be present in certain oxygen-rich shells (Henning et al. 1995). MgO, often known as *periclase*, is among the species that possess some of the highest dew points, which would enable it to nucleate at high temperatures. Could it then be the primary nucleating species in circumstellar clouds? Köhler, Gail & Sedlmayr (1997) investigated this possibility and eventually concluded that the nucleation rate of MgO would be too small in stellar environments for it to form stable dust seeds. It appeared that MgO vapour could be supercooled significantly, leading to a lower-than-expected condensation temperature, so that it no longer stood out on the basis of its high dew point temperature. The production rate of the condensed phase was low even for large degrees of supercooling since the work of formation of the critical cluster remained high. These calculations were based on a semi-empirical potential model that took into account several factors. These included the so-called T-Rittner potential, which considers polarizability of ions due to local electric fields in small clusters, and additional terms to account for a suspected covalent character in the Mg–O bonding.

However, it has been found that magnesium oxide requires a much more detailed potential model in order to correctly explain its experimental data ranging from the interionic distance to phonon dispersion curves. In this work, we therefore revisit the calculations of the critical work of formation of MgO, using a potential that is a combination of the 'compressible ion model' (CIM) and the 'polarizable ion model' (PIM) that was developed by Wilson and colleagues (Wilson & Madden 1996; Wilson, Pyper & Harding 1996b; Wilson 1997; Rowley et al. 1998). It is a sophisticated, transferable interionic potential designed to provide a better description of the properties of MgO clusters than any other models used in earlier studies. It not only considers the polarizability of ions, but also allows for changes in an ion's size and shape. The ions themselves are seen to be 'breathing' individually, making the model significantly more detailed than earlier models.

In the next section, the potential model of the previous studies by Köhler et al. is noted down for comparison and Section 3 summarizes the more accurate model of Wilson et al. The scheme for obtaining cluster-free energy is described in Section 4, followed by the results in Section 5.

2 POTENTIAL USED PREVIOUSLY

Some important issues regarding the molecular modelling of small MgO clusters have been discussed by Johnston (2003). Here, we briefly note the form of the MgO potential used in the earlier study of Köhler et al. (1997). Details such as numerical parameters are omitted here and can be found in the original publication.

Magnesium oxide is a highly ionic species when the interionic distance is close to equilibrium. Ionic crystals are usually described by the Born–Mayer (B–M) potential (Born & Mayer 1932), the simplest form of the potential energy being

$$U_{B-M} = \frac{1}{2}\sum_{\substack{\ell,j \\ \ell\neq j}} \frac{Q_\ell Q_j}{r_{\ell j}} + \frac{1}{2}\sum_{\substack{\ell,j \\ \ell\neq j}} A_{\ell j}\exp\left(-\frac{r_{\ell j}}{\rho_{\ell j}}\right). \quad (1)$$

The first summation represents Coulomb interaction between charges Q_ℓ and Q_j, situated at lattice sites labelled ℓ and j, respectively, and whose mutual separation is $r_{\ell j}$. The second summation quantifies the repulsion due to the overlap of the electron densities of two ions situated at ℓ and j. The parameter $A_{\ell j}$ is the strength of this repulsion and $\rho_{\ell j}$ measures how steep the repulsive potential is.

In the B–M potential, individual ions are considered to be spherical charged distributions packed together in a stable lattice configuration. For an infinitely large lattice with high symmetry, this may hold true since electric fields in the immediate vicinity of a given ion would cancel each other out. When one deals with small clusters, however, this symmetry is lost and hence each ion will experience a net electric field, which leads to the ion's polarization (Rittner 1951).

In addition to polarization effects, one also needs to keep in mind that the B–M potential is primarily useful for the purely ionic group I–VII compounds, whereas MgO is a group II–VI compound. The relatively moderate difference in the electronegativity of MgO ions seemed to suggest a significant contribution of covalent bonding (Pauling 1960), which may be described through the Morse potential.

Keeping in mind these two effects, the full potential employed in the previous work was

$$U_{Koh} = \sum_{\ell,j\text{ pairs}} \mathcal{A}e^{-\frac{2r_{\ell j}}{\rho}} - \sum_{\ell,j\text{ pairs}} \mathcal{B}e^{-\frac{r_{\ell j}}{\rho}}$$
$$+ \sum_{\ell,j\text{ pairs}} \frac{Q_\ell^{eff}Q_j^{eff}}{r_{\ell j}} - \sum_{\ell,j\text{ pairs}} \frac{Q_\ell^{eff}(\boldsymbol{\mu}_j\cdot\boldsymbol{r}_{\ell j})}{r_{\ell j}^3}, \quad (2)$$

where an effective charge Q_ℓ^{eff} is used rather than the bare charge Q_ℓ, due to the lower electronegativity difference of the ions in MgO (Ziemann & Castleman 1991). $\boldsymbol{\mu}_j$ is the induced dipole moment at the position of ion j, generated by the local electric field $\boldsymbol{E}_j$ due to all charges Q_k^{eff}, and can be expressed as

$$\boldsymbol{\mu}_j = \alpha_j\boldsymbol{E}_j = \alpha_j\sum_{\substack{k\\k\neq j}}\frac{Q_k^{eff}\boldsymbol{r}_{kj}}{r_{kj}^3}. \quad (3)$$

In equation (2), $\mathcal{A}$ and $\mathcal{B}$ are the scaling prefactors appearing in the Morse potential and are related to the depth of the potential.

3 POTENTIAL USED IN THIS WORK

The potential used for the present calculations is borrowed from a complex model that was developed through a series of publications (Wilson et al. 1996b; Wilson & Madden 1996; Wilson 1997; Rowley et al. 1998) in order to include a number of effects in MgO. The most radical of these is that individual ions are treated as compressible balls of charge distribution. This is a significant departure from the models described in the previous section, in which electron clouds of two neighbouring ions were allowed to overlap each other, but

the ions maintained their original identity in terms of ionic radii. The only way ionic shape deformation was allowed in the Rittner potential, for example, was through polarization effects in finite size (small) clusters. It is therefore often termed a 'rigid ion model' (RIM). In the CIM (Wilson et al. 1996b), the size of an ion is allowed to change via compression of its charge distribution, effected by the neighbouring ions. Polarization effects are then added through the PIM (Wilson & Madden 1996) and to further the refinement, there is also a scheme for allowing aspherical shape deformations of the ion (Rowley et al. 1998).

3.1 Compressible ion model

As the starting point of the CIM (Wilson et al. 1996b), the B–M potential is again used, but with a more elaborate form

$$
\begin{aligned}
U_{\text{B–M}} = &\frac{1}{2} \sum_{\substack{\ell,j \\ \ell \neq j}} \frac{Q_\ell Q_j}{r_{\ell j}} \\
&+ \frac{1}{2} \sum_{\substack{\ell,j \\ \ell \neq j}} A_{\ell j} \exp[-a_{\ell j}(r_{\ell j} - \sigma_\ell - \sigma_j)] \\
&- \frac{1}{2} \sum_{\substack{\ell,j \\ \ell \neq j}} \left[\frac{C_6^{\ell j}}{r_{\ell j}^6} f_6^{\ell j}(r_{\ell j}) + \frac{C_8^{\ell j}}{r_{\ell j}^8} f_8^{\ell j}(r_{\ell j}) \right]
\end{aligned}
\tag{4}
$$

$$
= U_{\text{Cou}} + U_{\text{rep}} + U_{\text{disp}}, \tag{5}
$$

that is, the potential is a sum of Coulombic attraction, short-range repulsion and an additional dispersion term. The repulsive potential in the second summation now includes ionic radii σ_ℓ and σ_j (cf. equation 1) and the range parameter, $a_{\ell j}$, characterizes the shape of the charge density. $C_6^{\ell j}$ and $C_8^{\ell j}$ are the dipole–dipole and dipole–quadrupole dispersion parameters, respectively, relevant to interaction between species ℓ and j. These can be derived from *ab initio* calculations or by experiments (Pyper 1986). $f_n^{\ell j}(r_{\ell j})$ are the damping functions to characterize the effect of the overlap of electron densities of ions ℓ and j and are represented by the so-called Tang–Toennies functions (Tang & Toennies 1984). When the overlap between two ions' wavefunctions is negligible, the damping functions are unity, but they drop towards zero as the overlap becomes significant. Hence, the functions $f_n^{\ell j}(r_{\ell j})$ reduce the effect of the dispersion terms in overlapping electron shells.

Ionic compression effects are accounted for by modifying the repulsive part of the potential, U_{rep} (second term of equation 4). In the CIM, the repulsive potential is a function of not only the ionic positions ($\{r_\ell\}_{\ell=1,N}$), where N is the total number of ions in the system, but also the change in the instantaneous ionic radii, $\delta\sigma_\ell$, with respect to some reference values $\bar{\sigma}_\ell$. Further, U_{rep} can be seen to be arising from two contributions: (i) the overlap between the electron clouds of two neighbouring ions (U_{ov}) and (ii) the energy it costs to deform each ion's electron density by the amount $\delta\sigma_\ell$, denoted by U_{self}. In other words,

$$
\begin{aligned}
U_{\text{rep}} \left(\{r_\ell, \delta\sigma_\ell\}_{\ell=1,N} \right) = &U_{\text{ov}} \left(\{r_\ell, \delta\sigma_\ell\}_{\ell=1,N} \right) \\
&+ U_{\text{self}} \left(\{r_\ell, \delta\sigma_\ell\}_{\ell=1,N} \right).
\end{aligned}
\tag{6}
$$

The simplest form for U_{ov} is

$$
\begin{aligned}
&U_{\text{ov}} \left(\{r_\ell, \delta\sigma_\ell\}_{\ell=1,N} \right) \\
&= \sum_{\ell,j \text{ pairs}} A_{\ell j} \exp\{-a_{\ell j} [r_{\ell j} - (\bar{\sigma}_\ell + \delta\sigma_\ell) - (\bar{\sigma}_j + \delta\sigma_j)]\}.
\end{aligned}
\tag{7}
$$

The Mg^{2+} ion is assumed to be electronically rigid compared to O^{2-} owing essentially to the electronegativity of the latter and also because the polarizability of Mg^{2+} is some three orders of magnitude smaller than that of O^{2-} in the crystal. A suitable form for U_{self} for an oxide ion is

$$
U_{\text{self}} \left(\{\delta\sigma_\ell\}_{\ell=1,N} \right) = \sum_\ell D \left(e^{\beta \, \delta\sigma_\ell} + e^{-\beta \, \delta\sigma_\ell} \right), \tag{8}
$$

where $2D$ is the energy of the reference ion without any compression ($\delta\sigma_\ell = 0$) and can be taken as the second electron affinity of oxygen (Harding & Pyper 1995). The parameter β is such that $D\beta^2$ is the harmonic force constant that resists the ion's breathing originating from the compression–decompression process.

3.2 Polarizable ion model

In this model, polarization effects are represented in a more realistic way than through the T-Rittner method. One has to not only consider polarization due to electric fields and field gradients due to the charges and dipole moments of neighbouring ions, but also the fact that as an ion's immediate neighbour moves off its lattice site, the shape of the confining potential changes. This in turn leads to additional short-range effects in the polarization potential energy. Furthermore, it turns out that the 'covalent' bond contribution suspected in the earlier work is merely a manifestation of thoroughly defined polarization effects (Wilson & Madden 1993, 1994).

In the PIM (Wilson, Madden & Costa-Cabral 1996a; Rowley et al. 1998), additional degrees of freedom (d.o.f.) are assigned to each ion ℓ alongside its position r_ℓ and the instantaneous change in its radius discussed in the CIM. These are the electric dipole moment $\mu_\ell = \{\mu_\ell^\alpha\}_{(\alpha=x,y,z)}$ and the quadrupole moment $\theta_\ell = \{\theta_\ell^{\alpha\beta}\}_{(\alpha\beta=xx,yy,zz,xy,xz,yz)}$. In other words, μ_ℓ has three components, whereas θ_ℓ has six, although $\theta_\ell^{\alpha\beta} = \theta_\ell^{\beta\alpha}$ implies that only five components of θ_ℓ are independent. The Greek superscripts α, β, etc., take on any of the Cartesian coordinate values x, y or z here. The dipole and quadrupole moments are now related to the local electric field via the relations (cf. equation 3):

$$
\mu_\ell^\alpha = \alpha^{\alpha\beta} E^\beta(r_\ell) + \frac{1}{3} B^{\alpha\beta,\,\gamma\delta} E^\beta(r_\ell) E^{\gamma\delta}(r_\ell) \tag{9}
$$

and

$$
\theta_\ell^{\alpha\beta} = \frac{1}{2} B^{\alpha\beta,\,\gamma\delta} E^\gamma(r_\ell) E^\delta(r_\ell) + C^{\alpha\beta\gamma\delta} E^{\gamma\delta}(r_\ell). \tag{10}
$$

Here, E^α and $E^{\alpha\beta}$ are components of the electric field and field gradient, respectively. α and C are the dipole and quadrupole polarizabilities and B is the dipole–dipole–quadrupole hyperpolarizability. After some elaborate analysis, it is possible to show (Buckingham 1967) that for a spherical ion, the components of α, C and B are determined by a single number.

The route to a generalized polarization potential is quite involved. However, it has been noted (Rowley et al. 1998) that for MgO, quadrupolar polarization effects are negligibly small in explaining phonon dispersion curves. Hence, if one considers only dipole effects, the polarization contribution can be written as

$$
\begin{aligned}
U_{\text{pol}} \left(\{r_\ell, \mu_\ell\}_{\ell=1,N} \right) = &\sum_{\ell,j \text{ pairs}} f^{(1)}(r_{\ell j}) \, Q_\ell T^{(1)}(r_{\ell j}) \cdot \mu_j \\
&+ \sum_{\ell,j \text{ pairs}} \mu_\ell T^{(2)}(r_{\ell j}) \cdot \mu_j \\
&+ \sum_\ell \left(\frac{1}{2} \right) k_\ell \, \mu_\ell^2.
\end{aligned}
\tag{11}
$$

The terms with k_ℓ represent the energy required to polarize the ion. The parameters k_ℓ are harmonic and anharmonic force constants and are related to polarizabilities α, C and B (Wilson et al. 1996a). $\boldsymbol{T}^{(1)}$ and $\boldsymbol{T}^{(2)}$ are the charge–dipole and dipole–dipole interaction tensors (Buckingham 1967), whose components are expressed, respectively, as

$$T_{\ell j}^\alpha = \nabla_\alpha \frac{1}{r_{\ell j}} \quad \text{and} \quad T_{\ell j}^{\alpha\beta} = \nabla_\alpha \nabla_\beta \frac{1}{r_{\ell j}}. \tag{12}$$

The radial function $f^{(1)}(r_{\ell j})$ modifies the interaction of charges with induced dipoles. It has a short-range effect only and is effective over length-scales of nearest-neighbour separations. These functions are generally chosen to be of the form of the Tang–Toennies dispersion damping function

$$f^{(n_k)}(r_{\ell j}) = 1 - e^{-br_{\ell j}} \sum_{k=0}^{n_k} \frac{(br_{\ell j})^k}{k!}, \tag{13}$$

where b is the reciprocal of the length-scale over which the damping is effective.

3.3 Aspherical ion model

The expressions for the repulsive potential given in equations (7) and (8) apply well for spherical compression of the ion. However, they still do not accurately reproduce desired phonon dispersion curves for MgO. For a better description of the interactions, one needs to consider aspherical ion deformation. For instance, an oxide ion is inhomogeneously compressed by a number of magnesium ions from different directions (maximum six neighbours) and the resulting shape of the O^{2-} ion would not be spherical. To incorporate aspherical compression, some modification of the repulsive potential is required. This is done by including yet more d.o.f. in terms of the parameters of dipole and quadrupole symmetry, $\boldsymbol{\nu}_\ell$ (3 d.o.f.) and $\boldsymbol{\kappa}_\ell$ (5 d.o.f.), which control the shape of the ion's repulsive wall. The 'aspherical ion model' (AIM) is an extension of the CIM in which U_{ov} and U_{self} take more complex forms. The cation–anion part of U_{ov} is generalized to

$$U_{ov}\left(\{\boldsymbol{r}_\ell, \delta\sigma_\ell, \boldsymbol{\nu}_\ell, \boldsymbol{\kappa}_\ell\}_{\ell=1,N}\right)$$
$$= \sum_{\ell \in \text{anion}} \sum_{j \in \text{cation}} A_{-+} \exp\left\{-a_{-+}\left[r_{\ell j} - (\bar\sigma_\ell + \delta\sigma_\ell) - (\bar\sigma_j)\right.\right.$$
$$\left.\left. - \boldsymbol{S}^{(1)}(\boldsymbol{r}_{\ell j}) \cdot \boldsymbol{\nu}_\ell - \boldsymbol{S}^{(2)}(\boldsymbol{r}_{\ell j}) \cdot \boldsymbol{\kappa}_\ell\right]\right\}, \tag{14}$$

where $\boldsymbol{S}^{(1)}$ and $\boldsymbol{S}^{(2)}$ are interaction tensors whose elements are given by

$$S_\alpha^{(1)}(\boldsymbol{r}) = \frac{r^\alpha}{r} \quad \text{and} \quad S_{\alpha\beta}^{(2)}(\boldsymbol{r}) = \frac{3\,r^\alpha r^\beta}{r^2} - \delta^{\alpha\beta}. \tag{15}$$

Here $\delta^{\alpha\beta}$ is the Kronecker delta. The self-energy of the CIM is generalized such that the energy required to cause the shape deformations of dipolar and quadrupolar symmetry is also considered:

$$U_{self}\left(\{\delta\sigma_\ell, \boldsymbol{\nu}_\ell, \boldsymbol{\kappa}_\ell\}_{\ell=1,N_{\text{anion}}}\right)$$
$$= \sum_{\ell \in \text{anion}} \left[D\left(e^{\beta\,\delta\sigma_\ell} + e^{-\beta\,\delta\sigma_\ell}\right) + \left(e^{\xi^2|\boldsymbol{\nu}^\ell|^2} - 1\right)\right.$$
$$\left. + \left(e^{\eta^2|\boldsymbol{\kappa}^\ell|^2} - 1\right)\right], \tag{16}$$

where ξ and η are two 'force constants' that can be chosen by noting high-symmetry points on the phonon dispersion curve. Here, we have assumed the cations Mg^{2+} to be non-compressible and

the asphericity effect on the O^{2-}–O^{2-} interactions has also been neglected since these effects have been found not to be influential in reproducing the observed phonon curves (Rowley et al. 1998). The variables $\boldsymbol{\nu}_\ell$ and $\boldsymbol{\kappa}_\ell$ minimize the total repulsive energy at each step of the molecular dynamics (MD) simulation.

3.4 Full potential for MgO

To recap, the CIM makes a number of modifications to the repulsive part of the potential in the B–M expression (4). In its simple form, the second term of equation (4) is replaced by equations (7) and (8), but if one considers details of dipolar and quadrupolar shape distortions, a combination of equations (14) and (16) would be more accurate. In addition, one needs to include the polarization potential, as given in equation (11).

Hence, the full potential for MgO, including all the compression, polarization and aspherical deformation effects, now reads

$$U_{\text{CIM+PIM}} = \sum_{\ell,j \text{ pairs}} \frac{Q_\ell Q_j}{r_{\ell j}}$$
$$- \sum_{\ell,j \text{ pairs}} \left[\frac{f_6^{\ell j}(r_{\ell j})C_6^{\ell j}}{r_{\ell j}^6} + \frac{f_8^{\ell j}(r_{\ell j})C_8^{\ell j}}{r_{\ell j}^8}\right]$$
$$+ U_{\text{rep}} + U_{\text{pol}}, \tag{17}$$

where

$$U_{\text{rep}} =$$
$$\sum_{\ell \in \text{anion}} \sum_{j \in \text{cation}} A_{-+} \exp\left\{-a_{-+}\left[r_{\ell j} - (\bar\sigma_\ell + \delta\sigma_\ell) - (\bar\sigma_j)\right.\right.$$
$$\left.\left. - \boldsymbol{S}^{(1)}(\boldsymbol{r}_{\ell j}) \cdot \boldsymbol{\nu}_\ell - \boldsymbol{S}^{(2)}(\boldsymbol{r}_{\ell j}) \cdot \boldsymbol{\kappa}_\ell\right]\right\}$$
$$+ \sum_{\ell \in \text{anion}} \left[D\left(e^{\beta\,\delta\sigma_\ell} + e^{-\beta\,\delta\sigma_\ell}\right)\right.$$
$$\left. + \left(e^{\xi^2|\boldsymbol{\nu}^\ell|^2} - 1\right) + \left(e^{\eta^2|\boldsymbol{\kappa}^\ell|^2} - 1\right)\right]. \tag{18}$$

and U_{pol} is given by equation (11).

4 FREE ENERGY CALCULATION

4.1 Statistical mechanics

The free energy of MgO clusters can be calculated by obtaining their harmonic frequencies using an MD simulation that employs the potential model described in the preceding section. These frequencies are then used in the equations of homogeneous nucleation (Ford 2004) some of which are summarized below.

Using expressions for the translational, rotational and vibrational partition functions (Z_{tran}, Z_{rot} and Z_{vib}, respectively), the Helmholtz free energy of a solid molecular cluster containing i diatomic monomers (such as MgO) can be expressed as

$$\mathcal{F}(i) = U_0(i) - k_B T \ln(Z_{\text{tran}} Z_{\text{rot}} Z_{\text{vib}})$$
$$= U_0(i) - k_B T \ln\left\{ V \left[\frac{2\pi\left(\sum_i m\right)k_B T}{h^2}\right]^{3/2} \frac{\pi^{1/2}}{\chi}\right.$$
$$\left.\left(\frac{8\pi^2 k_B T}{h^2}\right)^{3/2} (I_1 I_2 I_3)^{1/2} \prod_{k=1}^{6i-6} \frac{k_B T}{\hbar\omega_k}\right\}, \tag{19}$$

where $U_0(i)$ is the potential energy of the crystal at the mean atomic positions, k_B is Boltzmann's constant, T is the temperature, V is the volume of the container in which the cluster is able to translate freely, $\sum_i m$ denotes the cluster total mass, h is Planck constant, χ is the symmetry number associated with a given crystal geometry, I_1, I_2 and I_3 are the three principal moments of inertia of the cluster about the centre of mass when the atoms are in their mean positions and $\omega_k (k = 1, 2, \ldots, 6i - 6)$ are the angular frequencies of the vibrational modes (Abraham 1974; Mandl 1988).

In the bulk phase, the chemical potential of a single diatomic monomer of vapour is

$$\mu_v = U_0^{mon} - k_B T \ln \left[\frac{1}{\rho_v} \left(\frac{2\pi m k_B T}{h^2} \right)^{3/2} \right.$$

$$\left. \left(\frac{8\pi^2 k_B T}{h^2} I_{mon} \right) \frac{k_B T}{\hbar \omega_{mon}} \right], \tag{20}$$

where U_0^{mon} is the monomer's potential energy at the mean atomic positions, m is the monomer mass, ρ_v is the number density of the vapour monomers and is related to the vapour pressure p by $\rho_v k_B T = p$. The parameter I_{mon} is the moment of inertia of the monomer about its centre of mass and ω_{mon} is the angular frequency of the vibrational mode of the free monomer.

The work of formation of a crystal of size i from the vapour phase is

$$\mathcal{W}(i) = \mathcal{F}(i) - i\mu_v. \tag{21}$$

However, the expression for $\mathcal{W}(i)$ in equation (21) cannot be utilized directly if one wishes to calculate $\mathcal{W}(i)$ from an MD trajectory since the expression for $\mathcal{F}(i)$ contains volume V that must be eliminated. To solve this difficulty, it is useful to note that the nucleation rate is often written as

$$J = \mathcal{Z}\beta^* \exp\left(-\frac{\mathcal{W}^*}{k_B T} \right), \tag{22}$$

where β^* is the rate at which monomers are attached to a cluster of critical size i^*, $\mathcal{W}^*$ is the work of formation for the critical cluster size and $\mathcal{Z}$ is the dimensionless Zeldovich factor that is given by

$$\mathcal{Z} = \left[\frac{-1}{2\pi k_B T} \frac{d^2 \mathcal{W}(i)}{di^2} \right]^{1/2}. \tag{23}$$

The Zeldovich factor has been derived within the Becker–Döring framework of nucleation (Becker & Döring 1935) and equation (22) is not a result of the classical nucleation theory despite the appearance of an exponentiated free energy in it (Ford 2004). The calculated free energies may be used to derive the growth and decay rates that are used to specify the Becker–Döring equations. Equation (22) has been obtained by doing this and by solving the resulting Becker–Döring equations. The more elaborate Becker–Döring expression for nucleation rate is of the form

$$J = \frac{\beta_1 n_1}{1 + \sum_{i=2}^{i_{max}} \prod_{j=2}^{i} (\gamma_j / \beta_j)}, \tag{24}$$

where β_i is the rate at which molecules attach themselves to a cluster consisting of i monomers, γ_i is the rate at which molecules are lost from clusters of size i, n_1 is the mean population of monomers in the system and i_{max} is the largest cluster size considered in the system. In order to use expression (24), one requires to input the parameters β_i and γ_i for a range of cluster sizes, which may not necessarily be easy to obtain. The expression given in equation (22) circumvents this difficulty.

According to equation (22), the nucleation rate per unit volume is given by

$$J_V = \frac{J}{V} = \mathcal{Z}\beta^* \exp\left[-\frac{(\mathcal{W}^* + k_B T \ln V)}{k_B T} \right]$$

$$= \mathcal{Z}\beta^* \rho_v \exp\left[-\frac{(\mathcal{W}^* + k_B T \ln V)}{k_B T} - \ln\rho_v \right]. \tag{25}$$

On the other hand, the classical nucleation rate per unit volume can be written as

$$J_{V,clas} = \mathcal{Z}\beta^* \rho_v \exp\left(-\frac{\mathcal{W}^*_{clas}}{k_B T} \right). \tag{26}$$

Comparing equations (25) and (26) allows us to write the effective classical work of formation at the critical cluster size i^*, which can then be generalized for all cluster sizes as

$$\mathcal{W}_{eff}(i) = \mathcal{F}(i) - i\mu_v + k_B T \ln(\rho_v V). \tag{27}$$

From equation (19), it is apparent that $\mathcal{F}(i) + k_B T \ln V$ would be independent of the volume and knowledge of the number density of the vapour would thus allow us to estimate the work of formation using equations (19), (20) and (27).

The number of i-clusters per unit volume is given by

$$\rho_i = \frac{n_i}{V} = \exp\left[-\frac{(\mathcal{W}(i) + k_B T \ln V)}{k_B T} \right]. \tag{28}$$

The cluster population densities have been calculated according to a quasi-equilibrium expression using the calculated free energies. If the system were driven away from equilibrium, for instance by a very rapidly changing temperature, then corrections would be required. Nevertheless, the equilibrium populations are useful since they provide a clear picture for the onset conditions for nucleation. Calculations of the nucleation rate for a particular temperature history would in general require the solution to a set of kinetic Becker–Döring equations.

4.2 Molecular dynamics

An inspection of the relevant equations, particularly equations (19), (20) and (27), shows that in addition to the vapour density of MgO monomers, one needs to know the system potential energy at the mean atomic positions, $U_0(i)$, plus the mean ionic separations to calculate the moments of inertia, I_1, I_2 and I_3, plus the vibrational frequencies, ω_k, within the clusters. To obtain these quantities, the CIM + PIM potential was implemented using an MD simulation developed by Wilson et al., with the parameters appearing in the potential model chosen as in Wilson et al. (1996b), Wilson & Madden (1996), Wilson (1997) and Rowley et al. (1998).

In the bulk solid phase, MgO displays a simple cubic lattice structure of B1 type similar to NaCl (rocksalt), although it has been shown that for clusters smaller than 32 MgO monomers, nanotubes of stacked hexagons are energetically more favourable (Wilson 1997). To start with, in the MD simulation, some nominal lattice structure was chosen for a given cluster size and the structure was then relaxed by performing energy minimization through the steepest-descent method. The basic idea in this method is to follow the gradient of the potential energy surface through successive small steps until a minimum is found, that is to say, starting from the nominal lattice configuration, the vector

$$\nabla U = \left(\frac{\partial U}{\partial x_1}, \frac{\partial U}{\partial x_2}, \ldots, \frac{\partial U}{\partial x_{3N}} \right), \tag{29}$$

where $x_1, \ldots, x_{3N}$ are the ionic coordinates, is calculated. From this, a new set of ionic positions are calculated along the direction of $-\nabla U$ by calculating the new ionic coordinates

$$\left[\{\boldsymbol{r}_\ell\}_{\ell=1,N}\right]_{n+1} = \left[\{\boldsymbol{r}_\ell\}_{\ell=1,N}\right]_n - \Lambda_n \nabla U, \tag{30}$$

where the subscripts n and $n + 1$ denote two successive iterative steps and Λ_n is a small step size. This procedure is continued until a configuration corresponding to a minimum in the potential is found within a small tolerance. This may prove to be a slow procedure sometimes, in which case, conjugate gradient minimization may be performed (Press et al. 1992).

In such an energy-minimized configuration, U_0 is equal to the total energy of the cluster since the crystal has no kinetic energy and the interionic distances can also be measured easily in the absence of vibrational motion. The vibrational frequencies, ω_k, were then calculated by deriving the dynamical matrix of force constants from the relaxed structure. This was calculated in the MD simulation by displacing each ion of the relaxed lattice structure by a small amount one by one and measuring the force it experiences as a function of the displacement with respect to the relaxed position. It is assumed that the mutual force $F_{\ell j}$ experienced between the jth and the ℓth ion due to the displacement of the jth ion by an amount δx_j is governed by Hooke's law, written in tensorial form as

$$F_{\ell j}^\alpha = -k_{\ell j}^{\alpha\beta} \delta x_j^\beta, \tag{31}$$

where $k_{\ell j}^{\alpha\beta}$ is the spring constant. α and β here go from 1 to 3 and label the components of the force and displacement. In a system of N ions, each having 3 d.o.f., there will be $3N$ spring constants. Hence, the order of the dynamical matrix, **D**, which is composed of these spring constants, will be $3N$. One then finds the eigenvalues

λ_k of the mass-weighted dynamical matrix

$$\mathbf{D}' = \mathbf{M}^{-1/2} \mathbf{D} \mathbf{M}^{-1/2}, \tag{32}$$

where **M** is a diagonal matrix containing the masses of the $6i$ oscillators on its diagonal (Ashcroft & Mermin 1976).

The dynamical matrix, and hence **D**′, provides $6i$ eigenvalues in the case of a crystal with i molecules of MgO. However, six of them will, in principle, be zero because the modes corresponding to the entire crystal's translation in three dimensions plus rotation with respect to the three principal axes cannot contribute to the vibrational modes. Hence, we are left with $6i - 6$ non-zero eigenvalues of **D**′, except in the case of an isolated MgO monomer, which has one non-zero eigenvalue. The vibrational frequencies ω_k are related to these eigenvalues by

$$\omega_k = \sqrt{\lambda_k}, \tag{33}$$

which were used to obtain the vibrational free energy and eventually the total free energy of the MgO clusters using equation (19).

5 RESULTS AND DISCUSSION

Condensation of gaseous species around M stars is believed to occur somewhere in the temperature range of 800–1200 K and in the majority of cases, it is above 1000 K (Nuth & Donn 1982, 1983; Gail & Sedlmayr 1986, 1998). A number of possible cluster geometries containing up to 24 MgO monomers were considered, the relaxed structures of which are shown in Fig. 1. By calculating the free energy of each cluster as well as that of the monomer as discussed in Section 4, the effective work of formation of these clusters (equation 27) and the cluster number densities (equation 28) were evaluated as a function of their size i.
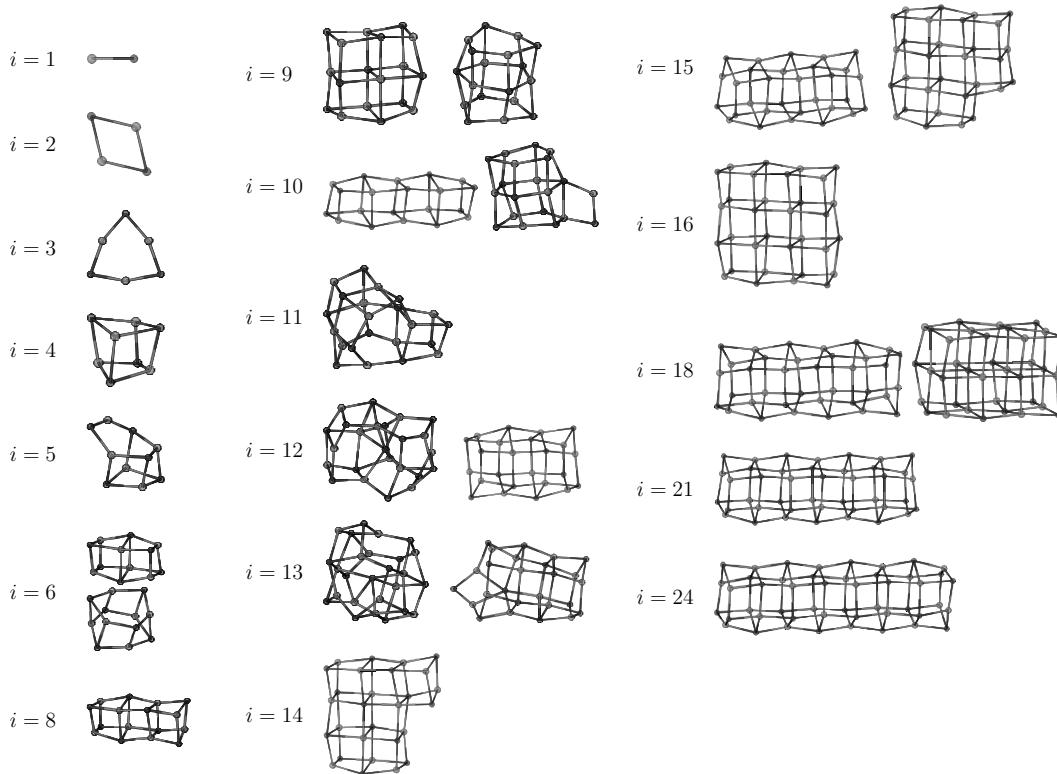

Figure 1. Various cluster geometries studied. Brighter balls are Mg^{2+} ions and the darker ones are O^{2-}.

The value of initial MgO vapour concentration was chosen to be $\rho_1 = 10^6$ m^{-3}, which is a typical value in shells surrounding M stars (Patzer, Köhler & Sedlmayr 1995; Köhler, Gail & Sedlmayr 1997). In a circumstellar outflow, this would not necessarily be the number density of MgO free monomers, for a vapour moving away from the central star will cool gradually and molecular clusters will be formed, consuming the free monomers and reducing their number density. Hence, an iterative method was used which ensured that the total density of MgO units remained constant even after considering the number densities of all the cluster sizes considered. We do this by taking a trial value of monomer density, ρ_v, and then evaluating the distribution ρ_i and calculating $\rho_{tot} = \rho_v + 2\rho_2 + 3\rho_3 + \ldots + i_{max}\rho_{i_{max}}$ using equation (28), where i_{max} is the largest cluster size considered ($i_{max} = 24$ in the present calculations). If ρ_{tot} does not match the desired value of ρ_1, we choose an improved trial value of ρ_v and continue to perform the calculation in this way until $\rho_{tot} \approx \rho_1$ within a small tolerance.

The effective work of formation obtained in this way for three different temperatures covering the range of interest is shown in Fig. 2, while Fig. 3 shows the corresponding distribution ρ_i. No distinct peak is visible in $\mathcal{W}_{eff}(i)$ and its value quickly rises to hundreds of $k_B T$, which indicates a lack of nucleation of MgO clusters in the given temperature range. This is also evident from the extremely small number densities for most cluster sizes, except for $i = 2$ and 3. The peak around these two sizes in Fig. 3 is a little unusual and suggests that MgO is an associative species, which prefers remain-
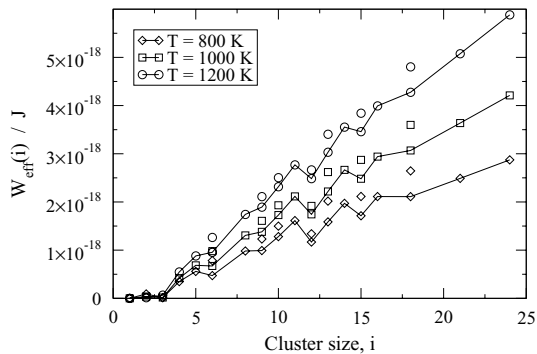

Figure 4. Number densities of various MgO cluster sizes as a function of temperature, with a fixed monomer concentration of 10^6 m^{-3}.

ing in clusters of (MgO)$_2$ and (MgO)$_3$ rather than as free monomers, at least under the circumstellar conditions mentioned above.

Fig. 4 shows how the number densities of clusters evolve as the circumstellar outflow moves away from the central star and cools down, assuming a constant vapour density. At around 1500 K, only monomers are predominant, but as the temperature drops, their concentration drops as (MgO)$_2$ and (MgO)$_3$ start to dominate. The total number density of MgO units remains fixed at 10^6 m^{-3} during the whole process.

What if the initial number density of MgO monomers were to be significantly greater than 10^6 m^{-3}? Fig. 5 shows the work of formation curves for two arbitrarily chosen higher values, $\rho_1 = 10^{15}$ m^{-3} and 10^{20} m^{-3}, each at the temperature $T = 800$ K, which is the lower limit of the temperature range of interest. For comparison, the $T = 800$ K curve from Fig. 2 has also been reproduced with these. The curve for $\rho_1 = 10^{15}$ m^{-3} does seem to be heading towards a peak value at some cluster size soon after $i = 25$, but the work of formation has already reached several dozens of $k_B T$ in the curve shown. The nucleation rate per unit volume, J_V, is proportional to $\exp(-\mathcal{W}^*/k_B T)$, where $\mathcal{W}^*$ is the peak value of $\mathcal{W}(i)$ (equation 25). Hence, nucleation in such a system would be expected to be an extremely inefficient process. Comparing this with the curve for $\rho_1 = 10^{20}$ m^{-3}, for which $\mathcal{W}^*$ appears to be very small (perhaps negative), it can be said that notable nucleation would only occur for initial vapour densities well above 10^{15} m^{-3}. Such MgO monomer concentrations are, however, atypical of circumstellar shells around oxygen-rich stars. Hence, MgO may be discarded as a candidate

Figure 2. Effective work of formation, , as a function of the MgO cluster size for various temperatures and a monomer concentration of 10^6 m^{-3}. The full line is drawn considering that the cluster which requires the least work of formation will be the most favoured among each size.
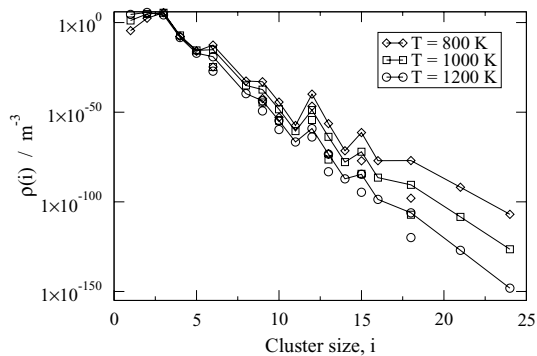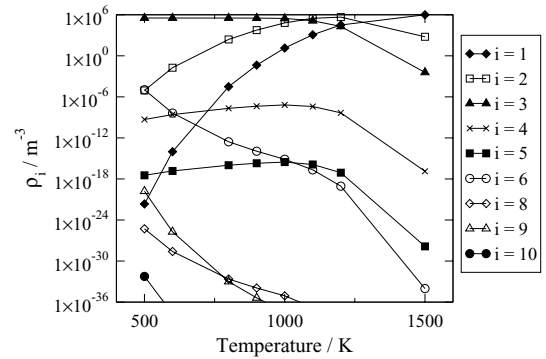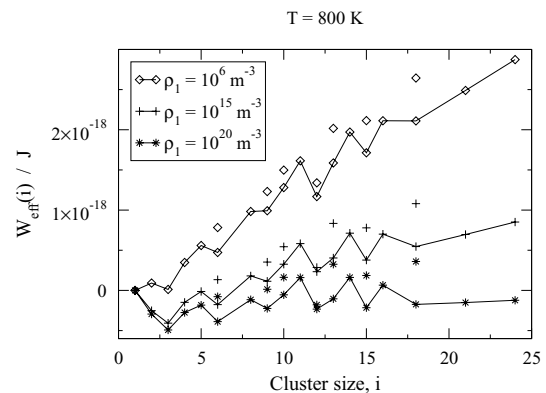

Figure 3. Distribution of the number densities of i-clusters for various temperatures and a monomer concentration of 10^6 m^{-3}. The full line connects the most-abundant clusters of each size.

Figure 5. Effective work of formation, , as a function of the MgO cluster size for various monomer concentrations, all at a fixed temperature of $T = 800$ K. The full line joins the clusters that require the least work of formation for each size.

for the primary nucleating species in stellar winds in those environments.

6 CONCLUSION

By utilizing the theory of homogeneous nucleation, we have explored the possibility that MgO could be the primary nucleating material in circumstellar shells around oxygen-rich M stars. To do this, a sophisticated potential model for MgO was used, which considers a number of details of the interactions within small MgO clusters. The model allows ionic shape deformations by modelling the compressibility of individual ions as well as considering non-vanishing polarization effects in small clusters. This model is much more complex than the ones previously used in similar studies of MgO.

Free energy calculations based on this model reveal that the work of formation required for the nucleation of MgO particles to occur is at least hundreds of $k_B T$ in the temperature range of 800–1200 K for an initial vapour density of 10^6 m^{-3}. Hence, MgO can be ruled out as a likely candidate for the primary nucleating dust species. It was found that meaningful nucleation rates for MgO would only be achieved in such a temperature range if the initial vapour density was much larger than some 10^{15} m^{-3}. However, such large concentrations of MgO are not found in oxygen-rich circumstellar shells.

The non-possibility of MgO nucleation is in agreement with a similar conclusion reached in earlier studies carried out with the help of a much simpler potential model (Köhler et al. 1997).

ACKNOWLEDGMENTS

REFERENCES

Abraham F. F., 1974, Homogeneous Nucleation Theory. Academic Press, New York
Ashcroft N. W., Mermin N. D., 1976, Solid State Physics. Saunders, Philadelphia
Becker R., Döring W., 1935, Ann. Phyz., Leipzig, 24, 719
Begemann B., Henning T., Mutschke H., Dorschner J., 1995, Planet. Space Sci., 43, 1257
Bhatt J. S., Ford I. J., 2003, J. Chem. Phys., 118, 3166
Born M., Mayer J. E., 1932, Zeitschr. f. Phys., 75, 1
Buckingham A. D., 1967, Adv. Chem. Phys., 12, 107
Cherchneff I., 2006, A&A, 456, 1001
Colangeli L. et al., 2003, A&AR, 11, 97
Dyson J. E., Williams D. A., 1997, The Physics of the Interstellar Medium. IOP Publishing, London
Ford I. J., 2004, Proc. Instn. Mech. Engrs., 218, 883
Gail H.-P., Sedlmayr E., 1985, A&A, 148, 183
Gail H.-P., Sedlmayr E., 1986, A&A, 166, 225
Gail H.-P., Sedlmayr E., 1987, in Morfill G. E., Scholer M., eds, Physical Processes in Interstellar Clouds. D. Reidel, Dordrecht
Gail H.-P., Sedlmayr E., 1988, A&A, 206, 153
Gail H.-P., Sedlmayr E., 1998, Faraday Discuss., 109, 303
Green N. J. B., Toniazzo T., Pilling M. J., Ruffle D. P., Bell N., Hartquist T. W., 2001, A&A, 375, 1111
Habing H. J., Olofsson H., eds, 2003, Asymptotic Giant Branch Stars. Springer-Verlag, New York
Harding J. H., Pyper N. C., 1995, Philos. Mag. Lett., 71, 113
Henning T., Begemann B., Mutschke H., Dorschner J., 1995, A&AS, 112, 143
Hoyle F., Wickramasinghe N. C., 1962, MNRAS, 124, 417
Johnston R. L., 2003, Dalton Trans., p. 4193
Köhler T. M., Gail H.-P., Sedlmayr E., 1997, A&A, 320, 553
Lushnikov A. A., Bhatt J. S., Ford I. J., 2003, J. Aerosol. Sci., 34, 1117
Mandl F., 1988, Statistical Physics, 2nd edn. Wiley, London
Molster F. J., Waters L. B. F. M., 2003, Astromineralogy, 609, 121
Nuth J. A., Donn B., 1982, J. Chem. Phys., 77, 2639
Nuth J. A., Donn B., 1983, J. Chem. Phys., 78, 1618
Patzer A. B. C., Köhler T. M., Sedlmayr E., 1995, Planet. Space Sci., 43, 1233
Pauling L., 1960, The Nature of the Chemical Bond and the Structure of Molecules and Crystals, 3rd edn. Cornell University Press, Ithaca
Press W. H., Teukolsky S. A., Vetterling W. T., Flannery B. P., 1992, Numerical Recipes, 2nd edn. Cambridge University Press, Cambridge
Pyper N. C., 1986, Phil. Trans. R. Soc. London A, 320, 107
Rittner E. S., 1951, J. Chem. Phys., 19, 1030
Rowley A. J., $\ddot{J}$ P., Wilson M., Madden P. A., 1998, J. Chem. Phys., 108, 10209
Tang K. T., Toennies J. P., 1984, J. Chem. Phys., 80, 3726
Tielens A. G. G. M., Waters L. B. F. M., Bernatowicz T. J., 2005, in Krot A. N., Scott E. R. D., Reipurth B., eds, ASP Conf. Ser. Vol. 341, Chondrites and the Protoplanetary Disk. Astron. Soc. Pac., San Francisco, p. 605
van Loon J. Th., Groenewegen M. A. T., de Koter A., Trams N. R., Waters L. B. F. M., Zijlstra A. A., Whitelock P. A., Loup C., 1999, A&A, 351, 559
Whittet D. C. B., 2003, Dust in the Galactic Environment, 2nd edn. IOP Publishing, London
Wilson M., 1997, J. Phys. Chem. B, 101, 4917
Wilson M., Madden P. A., 1993, J. Phys.: Condens. Matter, 5, 6833
Wilson M., Madden P. A., 1994, J. Phys.: Condens. Matter, 6, 159
Wilson M., Madden P. A., 1996, J. Phys. Chem., 100, 1227
Wilson M., Madden P. A., Costa-Cabral B. J., 1996a, J. Phys. Chem, 100, 1227
Wilson M., Pyper N. C., Harding J. H., 1996b, J. Chem. Phys., 104, 8068
Ziemann P. J., Castleman A. W., 1991, J. Chem. Phys., 94, 718

This paper has been typeset from a TEX/LATEX file prepared by the author.